Journal Pre-proof

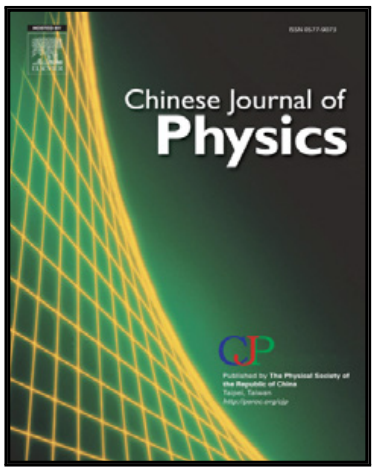

Germanium metasurface Near-Infrared High-Q absorber with symmetry-protected bound states in the continuum

Ming-Jyun Ye , Rashid G. Bikbaev , Dmitrii N. Maksimov , Pavel S. Pankin , Munho Kim , Ivan V. Timofeev , Kuo-Ping Chen

PII: S0577-9073(24)00319-8
DOI: https://doi.org/10.1016/j.cjph.2024.08.018
Reference: CJPH 2679

To appear in: *Chinese Journal of Physics*

Received date: 8 April 2024
Revised date: 12 July 2024
Accepted date: 13 August 2024

Please cite this article as: Ming-Jyun Ye , Rashid G. Bikbaev , Dmitrii N. Maksimov , Pavel S. Pankin , Munho Kim , Ivan V. Timofeev , Kuo-Ping Chen , Germanium metasurface Near-Infrared High-Q absorber with symmetry-protected bound states in the continuum, *Chinese Journal of Physics* (2024), doi: https://doi.org/10.1016/j.cjph.2024.08.018

Highlights

- The all-dielectric germanium metasurface absorber support simultaneous excitation of quasi bound state in the continuum (BIC) and super radiant mode.
- Trade-off metasurface between high Q-factor and high absorption in the photonic system could be selected via different hole depths in a germanium slab.
- The results are simulated and analyzed using the finite difference time domain (FDTD) and temporal coupled-mode theory (TCMT) method.
- After oblique incidence to break the symmetry, the excitation of the quasi-BIC allows to increase the absorptance by more than 4 times.
- The presented device demonstrated absorption of super radiant mode ~98.5% and quasi-BIC ~93% without back-metal reflector at the telecommunication wavelength.

Germanium metasurface Near-Infrared High-Q absorber with symmetry-protected bound states in the continuum

Ming-Jyun Ye[1], Rashid G. Bikbaev[2,3], Dmitrii N. Maksimov[2,3], Pavel S. Pankin[2,3*], Munho Kim[4], Ivan V. Timofeev[2,3] and Kuo-Ping Chen[5,1*]

[1] College of Photonics, National Chiao Tung University, 301 Gaofa 3rd Road, Tainan 711, Taiwan

[2] Kirensky Institute of Physics, Federal Research Center KSC SB RAS, Krasnoyarsk 660036, Russia

[3] Institute of Engineering Physics and Radioelectronics, Siberian Federal University, Krasnoyarsk 660041, Russia

[4] School of Electrical and Electronics Engineering, Nanyang Technological University, Singapore 639798, Singapore

[5] Institute of Photonics Technologies, National Tsing Hua University, Hsinchu, Taiwan

[*]Corresponding Author: pavel-s-pankin@iph.krasn.ru; kpchen@ee.nthu.edu.tw

ABSTRACT: The all-dielectric germanium nanohole (GNH) metasurface with a sub-wavelength thickness supports simultaneous excitation of quasi bound state in the continuum (BIC) and super radiant mode. By selecting the different hole depths in a germanium slab, we present a trade-off metasurface between high Q-factor and high absorption in the photonic system. The presented device demonstrated absorption of super-radiant mode ~98.5% and quasi-BIC ~93% without back-metal reflector at the telecommunication wavelength. The numerical results, obtained by the finite difference time domain (FDTD) method are explained in the framework of temporal coupled mode theory (TCMT).

KEYWORDS: *germanium (Ge), high-refractive index (HRI), dielectric, photodetector, metasurface, absorber*

Introduction

Typically, a photodetector employs an absorber which increases the photoelectron transformation efficiency in the specific spectral region. Higher efficiencies can be achieved by synthesizing new absorbing materials or using nanophotonic devices. Such artificially engineered nanophotonic devices, called metamaterials[1-7] or metasurfaces have been proposed in many applications, including broadband[6-8] and narrowband absorbers[9-11]. Due to their high-resolution detection properties, narrowband absorbers have been used in sensing and quantum optics[12-16]. The nanodevices can be composited with an ultrathin layer with high refractive index (HRI), providing strong field confinement matched with the intrinsic loss in the desired spectral range. The most promising HRI materials for metasurface design at the telecommunication wavelength are silicon (Si) and germanium (Ge). The germanium metasurface is more suitable for an absorber operating at wavelengths of around 1550 nm due to the large extinction coefficient.

The two major strategies for engineering the HRI metasurface absorbers are suppression of light scattering, namely the Kerker effect[17, 18], and application of optical bound states in the continuum (BICs) for critical field enhancement. The Kerker effect was proposed for electromagnetic scattering by magnetic spheres in 1983[19]. Compared to metal nanoparticles that only have an electric dipole (ED) distributed on the surface of the nanoparticle, both ED and a magnetic dipole (MD) resonances would be produced in the dielectric nanoparticle according to the Mie theory[18]. Under the proper conditions, the forward or backward scattering can be canceled by the destructive interference between the ED and MD resonances,

called the first- or second-type Kerker effect, respectively. Recently, the germanium metasurface absorber-based photodetector with 60% absorption was fabricated by using the lattice Kerker effect[20].

The BICs, leading to the other major strategy of HRI metasurface engineering, were initially proposed in quantum mechanics by von Neumann and Wigner[21]. The ideal BIC does not couple with the radiation channels, and cannot scatter incident light. In the last decade, quasi-BICs in photonic crystals, metasurfaces and waveguides have attracted extensive attention due to their interesting features, namely strong field confinement, and high Q-factor resonances[22-30,31]. The high Q-factor property has been applied for lasers[27, 28, 32, 33]and biosensors[34, 35] where the authors discussed that material loss, structure imperfection, or spectrometer resolution would limit the Q factor and figure of merit. However, there has been not much of discussion on harnessing the material loss near the semiconductor band edge with a BIC metasurface design in optoelectronics. In active optoelectronic dielectric metasurface, recent research used the conductive layer in manipulating liquid crystals[36, 37] and double electrodes[23] to achieve the tunable reflectance or transmittance resonances in visible range.

In recent years, some studies have discussed quasi-BICs (q-BICs) for absorption. They proposed the plasmonic q-BICs[22, 38-40] or hybrid metasurface q-BICs[22, 41-43] with a back-metal reflector. However, the plasmonic device and the back-metal reflector would produce unnecessary heat through intrinsic ohmic loss or thermal effect. Therefore, an all-dielectric metasurface absorber[44] provides essential development that opens tremendous opportunities in the sensing and detecting area. In previous research, Jianbo Yu et al. demonstrated an all-dielectric absorber with an absorptive dielectric germanium layer at ~1.2 um with the silicon metamirror[45]. In this study, we propose an all-dielectric germanium nanoholes (GNH) metasurface absorber based on excitation of high-Q quasi-BIC resonant mode near the symmetry-protected BIC (SP-BIC) simultaneously with the super radiant mode. This all dielectric GNH metasurface absorber can absorb up to 93% with Q-factor ~500 near the telecommunication wavelength 1550 nm.

RESULTS AND DISCUSSION

Design and optical characterization of the absorber.

The sketch view of the GNH metasurface absorber and its unit cell is shown in Figure 1(a). The lattice period P along the x and y axes is equal to 500 nm. The thickness H of the germanium film is 300 nm and the holes depth is *h*. The germanium film is located on a silicon dioxide (SiO_2) substrate. The refractive index and extinction coefficient of the Ge[46] are shown in Figure 1(b). The refractive index of the environment is equal to 1.5. The spectral properties of the proposed structure for different value of the remaining hole thickness (*H*-*h*) were calculated by the FDTD method. The GNH structure is illuminated from the top by a plane wave with E vector along the y-axis. The reflectance *R* and transmittance *T* are recorded at the top and bottom of the simulation box, respectively. Periodic boundary conditions are applied at the lateral boundaries of the simulation box, while the perfectly matched layer (PML) boundary conditions are used on the remaining interfaces at top and bottom. Absorptance *A* of the structure is determined by energy conservation law.

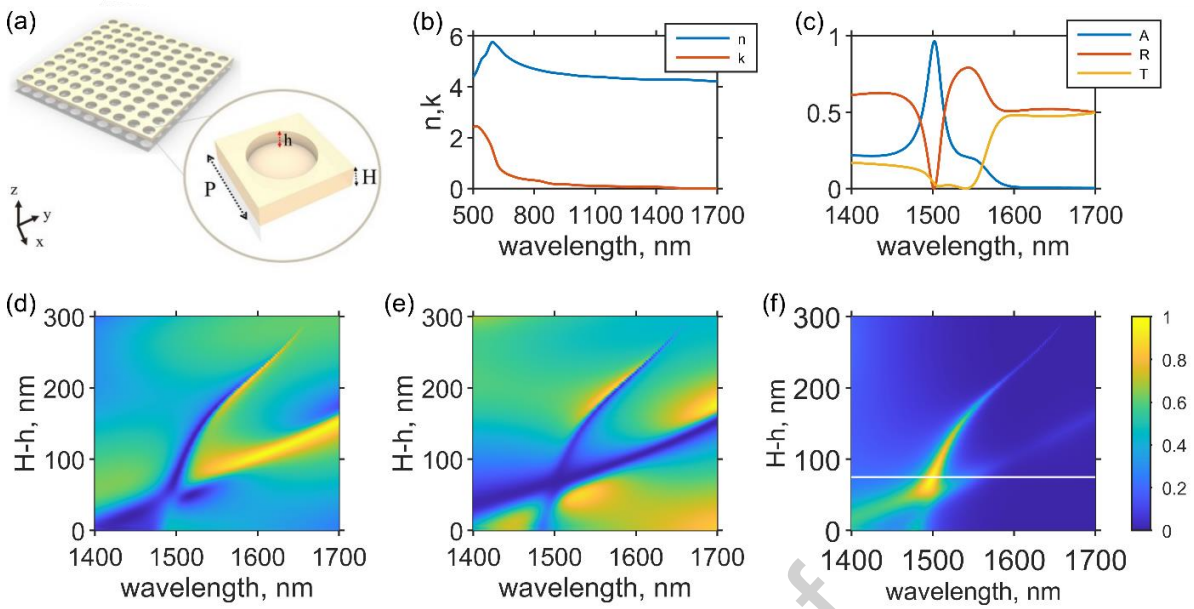

Figure 1. (a) Sketch view of the GNH absorber. (b) Refractive index and extinction coefficient of germanium. (c) Reflectance, transmittance and absorptance spectra of the GNH absorber for the remaining hole thickness H – h = 75 nm. (d) Reflectance, (e) transmittance and (f) absorptance spectra of the GNH absorber vs remaining hole thickness. White horizontal line corresponds to the value H – h = 75 nm.

It can be seen from Figure 1(d-f) that increasing the remaining hole thickness leads to avoided crossing of resonant lines in telecommunication wavelength region. As a result, reflectance and transmittance become close to zero, while absorption tends to unity. The absorptance reaches the maximal value equal to 98.5% with a remaining hole thickness H-h = 75 nm (white line at the Figure 1f). Corresponding spectra are shown in Figure 1(c). The Q-factor of the resonance near the maximum absorption point is calculated by solving the eigenvalue problem. The results are presented in Table 1. The small resonant Q-factors in Table 1 are due to material losses in Ge slab and significant radiation losses in the substrate and superstrate. If we want to enhance the Q-factor, get thicker remaining thickness from 75 to 80 nm, but the absorptance would decrease.

Table 1. Eigenfrequency, Q-factor, resonance wavelength and absorptance of the resonant mode for different values of the remaining hole thickness

remaining hole thickness (nm)	eigenfrequency (THz)	Q-factor	wavelength (nm)	absorptance (%)
70	200.04+1.9529i	51.215	1498.7	98
75	199.77+1.7778i	56.182	1500.7	98.5
80	199.54+1.6440i	60.689	1502.4	96.5

Since we cannot neglect the material losses in the GNH absorber, the excitation of high-Q resonances is possible only by controlling the radiation losses. In the case of BIC the radiation losses are equal to zero, as result the resonance cannot be excited either. The most common ways to excite a quasi-BIC include breaking the symmetry of the structure or the symmetry of the incident field. Tuning the parameters of the structure leads to a vanishing of the absorptance peak near 1500 nm. For this reason, the excitation of the quasi-BIC was achieved by breaking the symmetry of the incident field. The reflectance, transmittance and absorptance spectra of the structure for different values of the incident angle are shown in Figure 2(a-c). It can be seen from Figure 2(a-c) that the increase in the angle of incidence leads to the excitation of a quasi-BIC near 1550 nm. The reflectance and transmittance at the resonant wavelength decrease with the increase of the angle of incidence and become minimal at 1.7 degrees. At the same time,

the absorptance reaches the highest value of 93.5%. A further increase in the angle leads to drop in the absorptance.

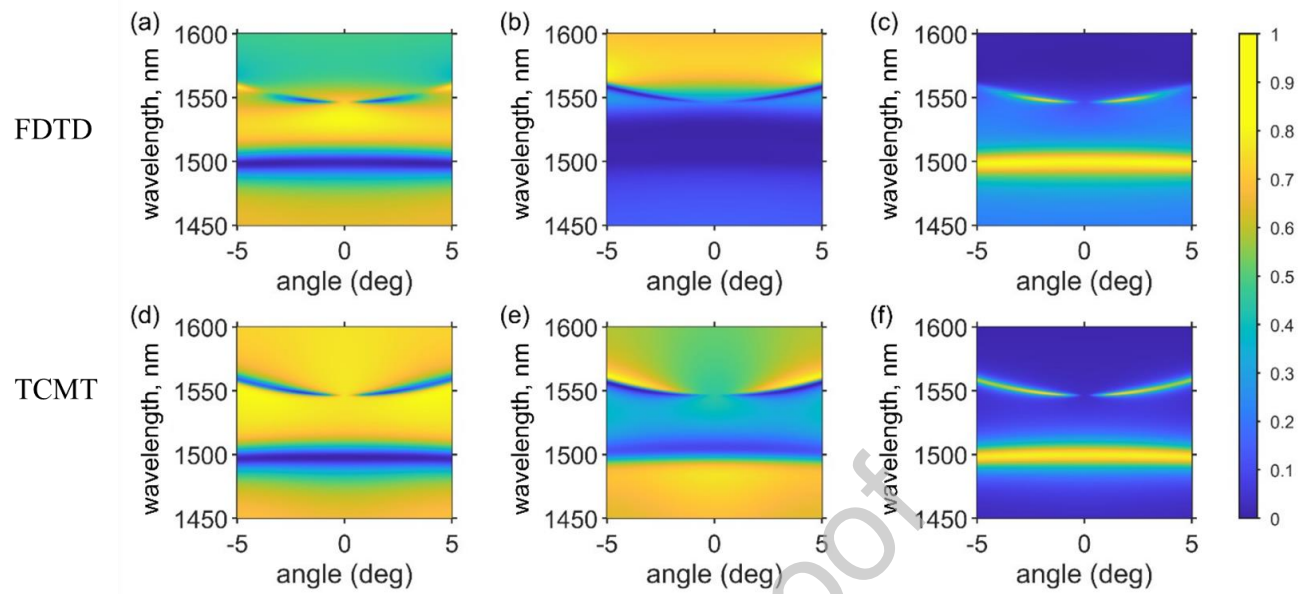

Figure 2. (a,d) Reflectance, (b,e) transmittance and (c,f) absorptance spectra of the GNH absorber simulated by (a-c) FDTD method and (e-f) TCMT vs angle of incidence. The TCMT model parameters are $\psi = \eta = 0, \rho = 0.8471, \tau = 0.5315$, $\alpha_1 = \alpha_2 = 0.1$, $\gamma_{01} = 0.0041, \gamma_{02} = 0.0137$, $\omega_{BIC} = 4.0631$, $\kappa_{\omega 1} = -0.0119$, $\kappa_{\gamma 1} = 0.006$, $\omega_{SR} = 4.1898$, $\kappa_{\omega 2} = 0.0016, \kappa_{\gamma 2}^{0} = 0.0142, \kappa_{\gamma 2} = -0.0021$.

Such behavior of the resonant mode can be explained in the framework of temporal coupled-mode theory (TCMT). Let us consider the GNH absorber as resonator system with two resonances and two physical ports. Each resonant mode is described by the amplitude a_n and complex eigenfrequency $\omega_{rn} = \omega_{0n} - i(\gamma_n + \gamma_{0n})$, n = 1,2. The imaginary part of the complex eigenfrequency consists of radiation decay rate γ_n and material loss decay rate γ_{0n}. For such a system, the dynamic equations in the framework of TCMT can be written as[47,48]

$$\frac{\partial}{\partial t}\begin{pmatrix} a_1 \\ a_2 \end{pmatrix} = -(i\hat{\Omega} + \hat{\Gamma} + \hat{\Gamma}_0)\begin{pmatrix} a_1 \\ a_2 \end{pmatrix} + \hat{D}^T \begin{pmatrix} s_1^{(+)} \\ s_2^{(+)} \end{pmatrix}, \qquad (1)$$

$$\hat{\Omega} = \begin{pmatrix} \omega_{01} & 0 \\ 0 & \omega_{02} \end{pmatrix}, \hat{\Gamma}_0 = \begin{pmatrix} \gamma_{01} & 0 \\ 0 & \gamma_{02} \end{pmatrix},$$

$$\begin{pmatrix} s_1^{(-)} \\ s_2^{(-)} \end{pmatrix} = \hat{C}\begin{pmatrix} s_1^{(+)} \\ s_2^{(+)} \end{pmatrix} + \hat{D}\begin{pmatrix} a_1 \\ a_2 \end{pmatrix}. \qquad (2)$$

Here $s_{\mathrm{m}}^{(\pm)}$ are the amplitudes of the plane waves in the ports with subscript m = 1, 2 corresponding to the upper and lower half-spaces, while superscripts $^{(+)}$,$^{(-)}$ stands for incident and outgoing waves, respectively. The direct (non-resonant) scattering process is described by the matrix $\hat{C}$

$$\hat{C} = e^{i\psi}\begin{pmatrix} \rho e^{-i\eta} & i\tau \\ i\tau & \rho e^{i\eta} \end{pmatrix}, \qquad (3)$$

where ψ, η, ρ, τ are real valued parameters such as $\rho^2 + \tau^2 = 1$. The matrix $\hat{D}$ contains the coupling constants d_{mn}

$$\hat{D} = \begin{pmatrix} d_{11} & d_{12} \\ d_{21} & d_{22} \end{pmatrix}.$$

There are two possibilities for the coupling constants column vectors[49]

$$\begin{pmatrix} d_{1\mathrm{n}} \\ d_{2\mathrm{n}} \end{pmatrix} = e^{i\frac{\psi}{2}} \sqrt{\frac{\gamma_{\mathrm{n}}}{1+\rho}} \begin{pmatrix} \left(\tau\sqrt{\alpha_{\mathrm{n}}} - i(1+\rho)\sqrt{1-\alpha_{\mathrm{n}}}\right) e^{-i\frac{\eta}{2}} \\ \left(\tau\sqrt{1-\alpha_{\mathrm{n}}} - i(1+\rho)\sqrt{\alpha_{\mathrm{n}}}\right) e^{i\frac{\eta}{2}} \end{pmatrix}, \qquad (4)$$

and

$$\begin{pmatrix} d_{1\mathrm{n}} \\ d_{2\mathrm{n}} \end{pmatrix} = e^{i\frac{\psi}{2}} \sqrt{\frac{\gamma_{\mathrm{n}}}{1+\rho}} \begin{pmatrix} \left(\tau\sqrt{\alpha_{\mathrm{n}}} + i(1+\rho)\sqrt{1-\alpha_{\mathrm{n}}}\right) e^{-i\frac{\eta}{2}} \\ \left(-\tau\sqrt{1-\alpha_{\mathrm{n}}} - i(1+\rho)\sqrt{\alpha_{\mathrm{n}}}\right) e^{i\frac{\eta}{2}} \end{pmatrix}, \qquad (5)$$

where $\alpha \in [0,1]$. The case $\alpha = 0$, $\tau = 0$ corresponds to an optical system decoupled from the lower half-space. The case $\alpha = 0.5$ applies to symmetric systems. In our case, the system is asymmetric. Thus, α is viewed as a fitting parameter. Assuming only the resonant absorption, when we can neglect an absorption in the direct process, matrix $\hat{\Gamma}$ can be found as

$$\hat{\Gamma} = 0.5\hat{D}^{\dagger}\hat{D}. \quad (6)$$

From Eq. (1), under a steady-state excitation $s_{1,2}^{(+)}(t) = e^{-i\omega t}$, the vector of the resonant modes amplitudes is

$$\begin{pmatrix} a_1 \\ a_2 \end{pmatrix} = \hat{A}^{-1}\hat{D} \begin{pmatrix} s_1^{(+)} \\ s_2^{(+)} \end{pmatrix}, \quad (7)$$

$$\hat{A} = i(\hat{\Omega} - \omega\hat{\mathbb{I}}) + \hat{\Gamma} + \hat{\Gamma}_0.$$

Using Eq. (7), the reflectance R and transmittance T can be found then directly from Eq. (2) as

$$R(\omega) \equiv \left|\frac{s_1^{(-)}}{s_1^{(+)}}\right|^2 = |C_{11} + d_{11}a_1 + d_{12}a_2|^2, \quad (8)$$

$$T(\omega) \equiv \left|\frac{s_2^{(-)}}{s_1^{(+)}}\right|^2 = |C_{21} + d_{21}a_1 + d_{22}a_2|^2. \quad (9)$$

The absorption can be found by its definition as

$$A(\omega) \equiv 2\gamma_{01}|a_1|^2 + 2\gamma_{02}|a_2|^2. \qquad (10)$$

We assumed that the system supports a symmetry protected BIC in the Γ-point. With variation of the angle of incidence θ the BIC is transformed to a high-Q resonance with the resonant frequency ω_{01} and the decay rate γ_1 given by the following equations,

$$\omega_{01}(\theta) = \omega_{BIC} + \kappa_{\omega 1}\theta^2 + \mathcal{O}(\theta^4),$$
$$\gamma_1(\theta) = \kappa_{\gamma 1}\theta^2 + \mathcal{O}(\theta^4), \quad (11)$$

where $\kappa_{\omega,\gamma}$ are the leading coefficients of the Taylor expansion. The similar expansions hold for the second superradiant resonant mode

$$\omega_{02}(\theta) = \omega_{SR} + \kappa_{\omega 2}\theta^2 + \mathcal{O}(\theta^4),$$
$$\gamma_2(\theta) = \kappa_{\gamma 2}^0 + \kappa_{\gamma 2}\theta^2 + \mathcal{O}(\theta^4). \quad (12)$$

Reflectance, transmittance and absorptance spectra calculated by Eqs. (8-10) are shown in Figure 2(d-f). It should be noted that results obtained by two different methods have a qualitative agreement.

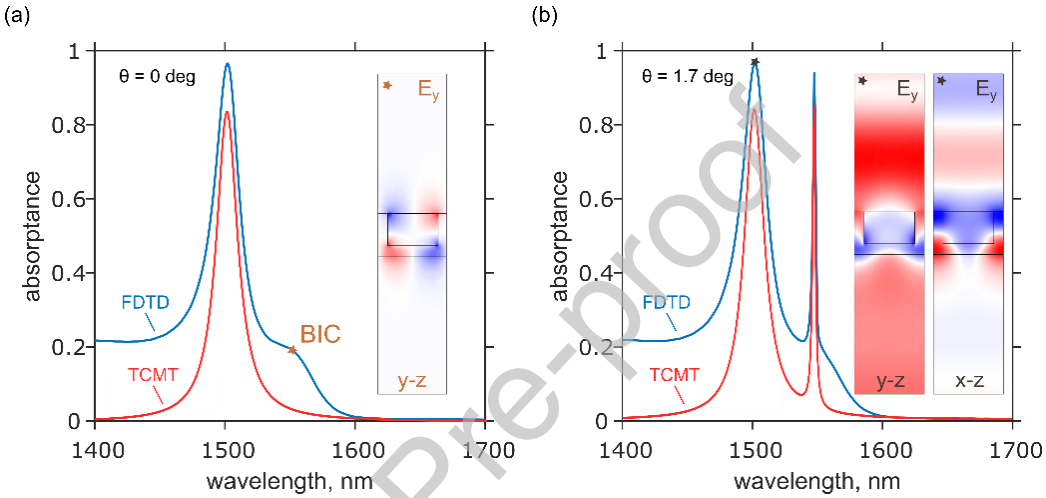

Figure 3. Absorptance spectra of the GNA for (a) θ = 0 deg and (b) θ = 1.7 deg.

The absorptance spectra of the structure for normal and oblique incidence and field distribution at BIC eigenmode and low Q-factor resonant eigenmode are shown in Figure 3. At θ = 0 the eigenmode field is localized about the nanohole array, which is a typical field distribution at Γ-point for SP-BIC, see Figure 3(a). The high absorption near 1500 nm is stimulated by the superradiant mode resonance independent of the incidence angle, as shown in Figure 3(b). The E_y-field of the superradiant resonant mode is not only present in the metasurface but in the substrate and the superstrate. The quantitative difference between two methods is seen. It stems due to the assumption of resonant absorption in TCMT method, i.e. the absorption in non-resonant (direct) process is taken as zero.

Table 2. Eigenfrequency, Q-factor, resonance wavelength and absorptance of the resonant mode for different angle of incidence

angle (deg)	eigenfrequency (THz)	Q-factor	wavelength (nm)	absorptance (%)
0	193.30+0.20754i	465.68	1550.9	19.5
1.7	193.10+0.19228i	502.12	1552.6	93.5

The eigenfrequencies, Q-factors and absorptance at the resonant wavelength for the θ = 0 and θ = 1.7 deg are presented in Table 2. The excitation of the quasi-BIC allows for an increase in absorptance by more than 4 times. Under oblique incidence, the Q-factor of the q-BIC mode achieves ~500, and it is ~9 times larger than the Q-factor of the superradiant mode. Thus, the energy is strongly confined inside the

GNH absorber at 1550 nm. This can find practical application in the design of devices for converting light energy into electrical energy such as photodetectors.

CONCLUSIONS

In summary, a symmetry-protected BIC metadevice with selective absorption and high Q-factors in the telecommunication wavelength is demonstrated via FDTD and TCMT methods. In the GNH absorber design, it is possible to reach the absorption up to 98.5% and trade off the high Q factor by modulating the remaining nanohole thickness without additional back reflector. After oblique incidence to break the symmetry, the excitation of the quasi-BIC allows to increase the absorptance by more than 4 times. Meanwhile, Q-factor of the q-BIC mode achieves ~500 and it is ~9 times larger than Q-factor of the superradiant mode.

Corresponding Author

*E-mail: pavel-s-pankin@iph.krasn.ru; kpchen@ee.nthu.edu.tw

Notes.

The authors declare no competing financial interest.

ACKNOWLEDGMENT

This work is supported by the National Science and Technology Council (NSTC; 111-2923-E-007-008-MY3; 111-2628-E-007-021; 112-2223-E-007 -007 -MY3; 112-2923-E-007 -004 -MY2; 112-2119-M-A49-008). This research was also funded by the Russian Science Foundation (project no. 22-42-08003).

References

1. Lv, H.; Yang, Z.; Xu, H.; Wang, L.; Wu, R., An electrical switch-driven flexible electromagnetic absorber. *Advanced Functional Materials* **2020,** *30* (4), 1907251.
2. Chen, K.; Adato, R.; Altug, H., Dual-band perfect absorber for multispectral plasmon-enhanced infrared spectroscopy. *ACS nano* **2012,** *6* (9), 7998-8006.
3. Shrekenhamer, D.; Chen, W.-C.; Padilla, W. J., Liquid crystal tunable metamaterial absorber. *Physical review letters* **2013,** *110* (17), 177403.
4. Landy, N. I.; Sajuyigbe, S.; Mock, J. J.; Smith, D. R.; Padilla, W. J., Perfect metamaterial absorber. *Physical review letters* **2008,** *100* (20), 207402.
5. Zhu, H.; Yi, F.; Cubukcu, E., Plasmonic metamaterial absorber for broadband manipulation of mechanical resonances. *Nature Photonics* **2016,** *10* (11), 709-714.
6. Zhou, Y.; Qin, Z.; Liang, Z.; Meng, D.; Xu, H.; Smith, D. R.; Liu, Y., Ultra-broadband metamaterial absorbers from long to very long infrared regime. *Light: Science & Applications* **2021,** *10* (1), 138.
7. Huang, Y.; Kaj, K.; Chen, C.; Yang, Z.; Ul Haque, S. R.; Zhang, Y.; Zhao, X.; Averitt, R. D.; Zhang, X., Broadband terahertz silicon membrane metasurface absorber. *ACS Photonics* **2022,** *9* (4), 1150-1156.
8. Lin, K.-T.; Chen, H.-L.; Lai, Y.-S.; Yu, C.-C., Silicon-based broadband antenna for high responsivity and polarization-insensitive photodetection at telecommunication wavelengths. *Nature communications* **2014,** *5* (1), 3288.
9. Tian, J.; Li, Q.; Belov, P. A.; Sinha, R. K.; Qian, W.; Qiu, M., High-Q all-dielectric metasurface: super and suppressed optical absorption. *Acs Photonics* **2020,** *7* (6), 1436-1443.
10. Shi, L.; Shang, J.; Liu, Z.; Li, Y.; Fu, G.; Liu, X.; Pan, P.; Luo, H.; Liu, G., Ultra-narrow multi-band polarization-insensitive plasmonic perfect absorber for sensing. *Nanotechnology* **2020,** *31* (46), 465501.

11. Yu, J.; Ma, B.; Qin, R.; Ghosh, P.; Qiu, M.; Li, Q., High-Q absorption in all-dielectric photonics assisted by metamirrors. *ACS Photonics* **2022,** *9* (10), 3391-3397.
12. Saha, S.; Ozlu, M. G.; Chowdhury, S. N.; Diroll, B. T.; Schaller, R. D.; Kildishev, A.; Boltasseva, A.; Shalaev, V. M., Tailoring the Thickness-Dependent Optical Properties of Conducting Nitrides and Oxides for Epsilon-Near-Zero-Enhanced Photonic Applications. *Advanced Materials* **2022**, 2109546.
13. Ghafari, B.; Danaie, M.; Afsahi, M., Perfect Absorber Based on Epsilon-Near-Zero Metamaterial as a Refractive Index Sensor. *Sensing and Imaging* **2023,** *24* (1), 15.
14. Akhlaghi, M. K.; Schelew, E.; Young, J. F., Waveguide integrated superconducting single-photon detectors implemented as near-perfect absorbers of coherent radiation. *Nature communications* **2015,** *6* (1), 8233.
15. Zhang, J.; MacDonald, K. F.; Zheludev, N. I., Controlling light-with-light without nonlinearity. *Light: Science & Applications* **2012,** *1* (7), e18-e18.
16. Vassant, S.; Hugonin, J.-P.; Marquier, F.; Greffet, J.-J., Berreman mode and epsilon near zero mode. *Optics express* **2012,** *20* (21), 23971-23977.
17. Yang, C.-Y.; Yang, J.-H.; Yang, Z.-Y.; Zhou, Z.-X.; Sun, M.-G.; Babicheva, V. E.; Chen, K.-P., Nonradiating silicon nanoantenna metasurfaces as narrowband absorbers. *Acs Photonics* **2018,** *5* (7), 2596-2601.
18. Babicheva, V. E.; Evlyukhin, A. B., Resonant lattice Kerker effect in metasurfaces with electric and magnetic optical responses. *Laser & Photonics Reviews* **2017,** *11* (6), 1700132.
19. Kerker, M.; Wang, D.-S.; Giles, C., Electromagnetic scattering by magnetic spheres. *JOSA* **1983,** *73* (6), 765-767.
20. Zhou, Z.-X.; Ye, M.-J.; Yu, M.-W.; Yang, J.-H.; Su, K.-L.; Yang, C.-C.; Lin, C.-Y.; Babicheva, V. E.; Timofeev, I. V.; Chen, K.-P., Germanium metasurfaces with lattice kerker effect in near-infrared photodetectors. *ACS nano* **2022,** *16* (4), 5994-6001.
21. von Neuman, J.; Wigner, E., Uber merkwürdige diskrete Eigenwerte. Uber das Verhalten von Eigenwerten bei adiabatischen Prozessen. *Physikalische Zeitschrift* **1929,** *30*, 467-470.
22. Azzam, S. I.; Shalaev, V. M.; Boltasseva, A.; Kildishev, A. V., Formation of bound states in the continuum in hybrid plasmonic-photonic systems. *Physical review letters* **2018,** *121* (25), 253901.
23. Sun, K.; Wei, H.; Chen, W.; Chen, Y.; Cai, Y.; Qiu, C.-W.; Han, Z., Infinite-Q guided modes radiate in the continuum. *Physical Review B* **2023,** *107* (11), 115415.
24. Wu, B. R.; Yang, J. H.; Pankin, P. S.; Huang, C. H.; Lee, W.; Maksimov, D. N.; Timofeev, I. V.; Chen, K. P., Quasi-Bound States in the Continuum with Temperature-Tunable Q Factors and Critical Coupling Point at Brewster's Angle. *Laser & Photonics Reviews* **2021,** *15* (5), 2000290.
25. Bogdanov, A. A.; Koshelev, K. L.; Kapitanova, P. V.; Rybin, M. V.; Gladyshev, S. A.; Sadrieva, Z. F.; Samusev, K. B.; Kivshar, Y. S.; Limonov, M. F., Bound states in the continuum and Fano resonances in the strong mode coupling regime. *Advanced Photonics* **2019,** *1* (1), 016001-016001.
26. Gansch, R.; Kalchmair, S.; Genevet, P.; Zederbauer, T.; Detz, H.; Andrews, A. M.; Schrenk, W.; Capasso, F.; Lončar, M.; Strasser, G., Measurement of bound states in the continuum by a detector embedded in a photonic crystal. *Light: Science & Applications* **2016,** *5* (9), e16147-e16147.
27. Hwang, M.-S.; Lee, H.-C.; Kim, K.-H.; Jeong, K.-Y.; Kwon, S.-H.; Koshelev, K.; Kivshar, Y.; Park, H.-G., Ultralow-threshold laser using super-bound states in the continuum. *Nature Communications* **2021,** *12* (1), 4135.
28. Yang, J. H.; Huang, Z. T.; Maksimov, D. N.; Pankin, P. S.; Timofeev, I. V.; Hong, K. B.; Li, H.; Chen, J. W.; Hsu, C. Y.; Liu, Y. Y., Low-threshold bound state in the continuum lasers in hybrid lattice resonance metasurfaces. *Laser & Photonics Reviews* **2021,** *15* (10), 2100118.
29. Murai, S.; Abujetas, D. R.; Liu, L.; Castellanos, G. W.; Giannini, V.; Sánchez-Gil, J. A.; Tanaka, K.; Gómez Rivas, J., Engineering bound states in the continuum at telecom wavelengths with non-bravais lattices. *Laser & Photonics Reviews* **2022,** *16* (11), 2100661.
30. Liu, M.; Choi, D.-Y., Extreme Huygens' metasurfaces based on quasi-bound states in the continuum. *Nano letters* **2018,** *18* (12), 8062-8069.

31. Rybin, M. V.; Koshelev, K. L.; Sadrieva, Z. F.; Samusev, K. B.; Bogdanov, A. A.; Limonov, M. F.; Kivshar, Y. S., High-Q supercavity modes in subwavelength dielectric resonators. *Physical review letters* **2017,** *119* (24), 243901.
32. Rybin, M.; Kivshar, Y., Supercavity lasing. *Nature* **2017,** *541* (7636), 164-165.
33. Chen, M. H.; Xing, D.; Su, V. C.; Lee, Y. C.; Ho, Y. L.; Delaunay, J. J., GaN Ultraviolet Laser based on Bound States in the Continuum (BIC). *Advanced Optical Materials* **2023,** *11* (6), 2201906.
34. Wang, J.; Kühne, J.; Karamanos, T.; Rockstuhl, C.; Maier, S. A.; Tittl, A., All-dielectric crescent metasurface sensor driven by bound states in the continuum. *Advanced Functional Materials* **2021,** *31* (46), 2104652.
35. Ding, J.; Huang, L.; Luo, Y.; Wang, T.; Hu, J.; Li, R.; Xiao, S., Multi-Band Polarization-Independent Quasi-Bound States in the Continuum Based on Tetramer-Based Metasurfaces and Their Potential Application in Terahertz Microfluidic Biosensing. *Advanced Optical Materials* **2023**, 2300685.
36. Sun, M.; Xu, X.; Sun, X. W.; Liang, X. a.; Valuckas, V.; Zheng, Y.; Paniagua-Domínguez, R.; Kuznetsov, A. I., Efficient visible light modulation based on electrically tunable all dielectric metasurfaces embedded in thin-layer nematic liquid crystals. *Scientific reports* **2019,** *9* (1), 8673.
37. Zou, C.; Amaya, C.; Fasold, S.; Muravsky, A. A.; Murauski, A. A.; Pertsch, T.; Staude, I., Multiresponsive dielectric metasurfaces. *ACS Photonics* **2021,** *8* (6), 1775-1783.
38. Joseph, S.; Sarkar, S.; Khan, S.; Joseph, J., Exploring the optical bound state in the continuum in a dielectric grating coupled plasmonic hybrid system. *Advanced Optical Materials* **2021,** *9* (8), 2001895.
39. Aigner, A.; Tittl, A.; Wang, J.; Weber, T.; Kivshar, Y.; Maier, S. A.; Ren, H., Plasmonic bound states in the continuum to tailor light-matter coupling. *Science advances* **2022,** *8* (49), eadd4816.
40. Tang, Y.; Liang, Y.; Yao, J.; Chen, M. K.; Lin, S.; Wang, Z.; Zhang, J.; Huang, X. G.; Yu, C.; Tsai, D. P., Chiral bound states in the continuum in plasmonic metasurfaces. *Laser & Photonics Reviews* **2023,** *17* (4), 2200597.
41. Wang, H.; Zhou, J.; Song, D.; Wang, Y., Active tuning of near-infrared electromagnetic responses in the graphene/silicon hybrid nanohole arrays by electrical control. *Physical Review B* **2022,** *105* (3), 035407.
42. Jin, R.; Huang, L.; Zhou, C.; Guo, J.; Fu, Z.; Chen, J.; Wang, J.; Li, X.; Yu, F.; Chen, J., Toroidal dipole BIC-driven highly robust perfect absorption with a graphene-loaded metasurface. *Nano Letters* **2023,** *23* (19), 9105-9113.
43. Masoudian Saadabad, R.; Huang, L.; Miroshnichenko, A. E., Polarization-independent perfect absorber enabled by quasibound states in the continuum. *Physical Review B* **2021,** *104* (23), 235405.
44. Bikbaev, R. G.; Maksimov, D. N.; Pankin, P. S.; Ye, M.-J.; Chen, K.-P.; Timofeev, I. V., Enhanced light absorption in Tamm metasurface with a bound state in the continuum. *Photonics and Nanostructures-Fundamentals and Applications* **2023,** *55*, 101148.
45. Yu, J.; Ma, B.; Ouyang, A.; Ghosh, P.; Luo, H.; Pattanayak, A.; Kaur, S.; Qiu, M.; Belov, P.; Li, Q., Dielectric super-absorbing metasurfaces via PT symmetry breaking. *Optica* **2021,** *8* (10), 1290-1295.
46. Palik, E. D. In *Handbook of optical constants of solids*; Academic press: 1998; Vol. 3.
47. Fan, S.; Suh, W.; Joannopoulos, J. D., Temporal coupled-mode theory for the Fano resonance in optical resonators. *JOSA A* **2003,** *20* (3), 569-572.
48. Suh, W.; Wang, Z.; Fan, S., Temporal coupled-mode theory and the presence of non-orthogonal modes in lossless multimode cavities. *IEEE Journal of Quantum Electronics* **2004,** *40* (10), 1511-1518.
49. Maksimov, D. N.; Bogdanov, A. A.; Bulgakov, E. N., Optical bistability with bound states in the continuum in dielectric gratings. *Physical Review A* **2020,** *102* (3), 033511.

Graphical Abstract

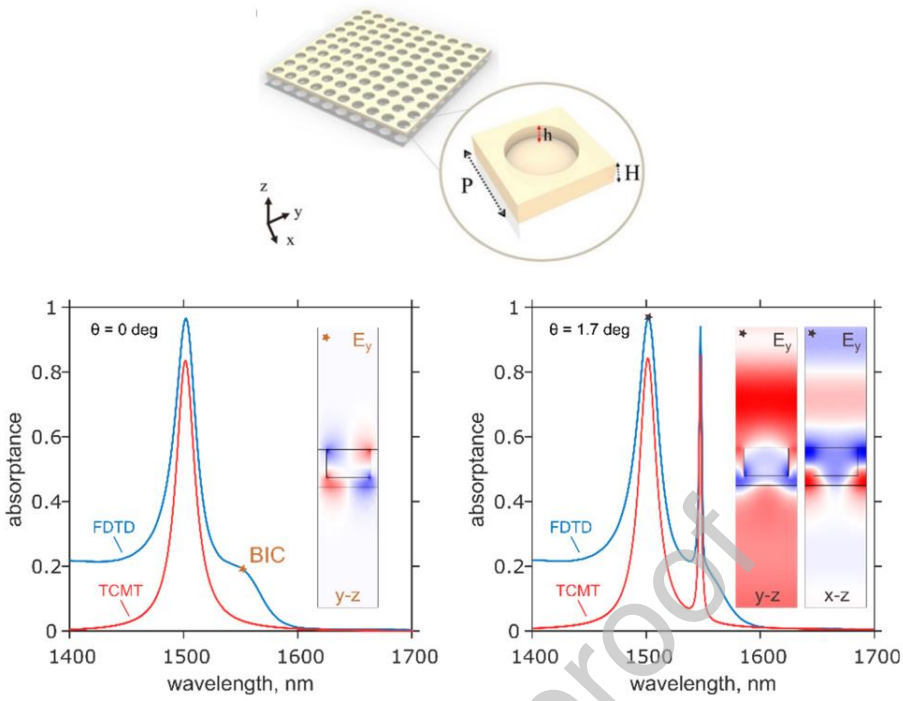

Declaration of interests

☒ The authors declare that they have no known competing financial interests or personal relationships that could have appeared to influence the work reported in this paper.

☒ The author is an Editorial Board Member/Editor-in-Chief/Associate Editor/Guest Editor for *[Chinese Journal of Physics]* and was not involved in the editorial review or the decision to publish this article.

☐ The authors declare the following financial interests/personal relationships which may be considered as potential competing interests: